

PAPER

The impact of carbon and oxygen in alpha-titanium: *ab initio* study of solution enthalpies and grain boundary segregation

To cite this article: D A Aksyonov *et al* 2016 *J. Phys.: Condens. Matter* **28** 385001

View the [article online](#) for updates and enhancements.

Related content

- [Grain boundary segregation of C, N and O in hexagonal close-packed titanium from first principles](#)
D A Aksyonov, A G Lipnitskii and Yu R Kolobov
- [Ab initio study of H, He, Li and Be impurity effect in tungsten and grain boundaries](#)
Wahyu Setyawan and Richard J Kurtz
- [Si segregation at Fe grain boundaries analyzed by ab initio local energy and local stress](#)
Somesh Kr Bhattacharya, Masanori Kohyama, Shingo Tanaka *et al*.

Recent citations

- [Interaction of Ti and Cr atoms with point defects in bcc vanadium: A DFT study](#)
A.O. Boev *et al*



IOP | ebooks™

Bringing you innovative digital publishing with leading voices to create your essential collection of books in STEM research.

Start exploring the collection - download the first chapter of every title for free.

The impact of carbon and oxygen in alpha-titanium: *ab initio* study of solution enthalpies and grain boundary segregation

D A Aksyonov^{1,2}, T Hickel¹, J Neugebauer¹ and A G Lipnitskii²

¹ Max-Planck-Institut für Eisenforschung GmbH, Max-Planck-Str. 1, 40237 Düsseldorf, Germany

² The Center of Nanostructured Materials and Nanotechnologies, Belgorod State University, Belgorod, Russian Federation

E-mail: dimonaks@gmail.com

Received 4 April 2016, revised 30 June 2016

Accepted for publication 6 July 2016


Published 27 July 2016



Abstract

The solution, grain boundary (GB) segregation, and co-segregation of carbon and oxygen atoms in α -titanium are studied using density functional theory. For five titanium tilt boundaries, including T1, T2, and C1 twin systems, we determine the GB structure, as well as GB energy and excess volume. The segregation energies and volumes of carbon and oxygen are calculated for 23 inequivalent interstitial voids, while for co-segregation 75 configurations are considered. It is obtained that depending on the type of the segregation void both a positive and a negative segregation process is possible. The physical reasons of segregation are explained in terms of the analysis of the void atomic geometry, excess volume and features of the electronic structure at the Fermi level. Although carbon and oxygen show qualitatively similar properties in α -Ti, several distinctions are observed for their segregation behavior and mutual interactions.

Keywords: grain boundary segregation, titanium, first-principles

 Online supplementary data available from stacks.iop.org/JPhysCM/28/385001/mmedia

(Some figures may appear in colour only in the online journal)

1. Introduction

Pure titanium with a nanocrystalline structure (nTi) is a promising material for many applications, as for example manufacturing of human dental implants [1, 2]. In addition to its excellent biocompatibility and strength, due to the relatively immobile grain boundaries (GB) which prevent the coarsening of nano-grains, nTi has a satisfactory thermal stability [3–5]. However, the particular mechanisms of grain boundary stabilization are still unclear.

The hexagonal closed-packed (hcp) and body-centered cubic (bcc) crystal structures of pure titanium, which are known as α -Ti and β -Ti (above 1156 K), respectively, determine the variety of titanium alloys. Among them commercially pure α -Ti (CP-Ti) and classical $\alpha + \beta$ Ti-6Al-4V

alloys, where the α phase is prevalent, cover up to 80% of the metallic Ti usage [6].

The main difference between the commercial grades 1–4 of CP-Ti materials is their amount of oxygen. Despite the small concentrations, oxygen has a pronounced influence on Ti properties. For example, the increase of oxygen content from 0.18 wt.% in a grade 1 to 0.25 wt.% in a grade 2 material results in an improvement of yield strength from 220 MPa up to 400 MPa. More important for the present study is the fact that alloys with higher oxygen concentrations have a better thermal stability of the GB structure [7]. A possible reason of stabilization can be the GB segregation of O atoms and the accompanied reduction of GB energy and mobility—an effect that has been earlier discovered in several metallic alloys [8].

Indeed, an increased concentration of oxygen at GBs was observed experimentally in CP-Ti by atom probe tomography [9]. Nevertheless, the existence of an equilibrium GB segregation of O in Ti remains questionable. It was shown from first principles that O can be attracted by basal stacking faults [10] and twin boundaries [11], and repelled by high angle GBs [12] and prismatic stacking faults [11]. However, the physical reasons for such behavior are still not fully resolved.

The influence of carbon on the materials strength is comparable to that of oxygen [7], however, the actual concentrations of C in CP-Ti alloys are much smaller and lie in the region of 0.02–0.08 wt.% [4, 13–15]. It is traditionally considered that the presence of more than 0.1 wt.% of C causes the formation of Ti-C carbide particles and leads to embrittlement of coarse-grained Ti [16]. At the same time the GB segregation of C is also possible [9], but it is studied in less degree than for the case of O.

Finally, the details of mutual interaction between C and O in Ti are not studied at all. In particular, it is unclear whether a co-segregation or just a competitive segregation of C and O was observed experimentally [9]. Since the segregation depends on the chemical potentials of C and O in the bulk of Ti, the details of their pair interaction in solid solution have the same importance as their possible co-segregation at GBs.

In the present study we have therefore investigated the interaction of C and O in bulk Ti and at GBs for the case of hexagonal close-packed (hcp) α -Ti using density functional theory (DFT). The choice of GBs and calculation of their energies is made in section 3. Sections 4 and 6 are devoted to the study of impurity interactions in bulk Ti. The main emphasis is made upon the study of C and O segregation (section 5) and their co-segregation (section 7) at GBs.

2. Computational details

Calculations of the full energies and optimized geometries were performed using the DFT framework [17, 18] within the generalized gradient approximation (GGA), the Perdew–Burke–Ernzerhof (PBE) functional [19] and projected augmented wave (PAW) method [20] (VASP [21]). We considered the following valence electronic states: 3s, 3p, 4s, 3d for Ti and 2s, 2p for C and O.

An energy cut-off of 441 eV for the plane-wave basis set ensures energy convergence on the order of 3 meV/atom and allows us to determine lattice constants with 0.004 Å and 0.007 Å precision for a and c . The Brillouin-zone integrals were approximated using the special k-point sampling of Monkhorst and Pack [22] with densities of k-points of 0.2–0.25 Å^{−3}. We used Methfessel-Paxton [23] smearing for Brillouin-zone integration with a smearing width of 0.2 eV. Such density of k-points and value of smearing ensures convergence of 0.1 meV/atom for energy, and 0.002 Å and 0.005 Å for a and c lattice parameters. The structural optimization was performed until the forces acting on each atom were less than 25 meV Å^{−1}.

The calculations were performed under three-dimensional periodic boundary conditions (PBC). For each considered GB two types of supercells were constructed: (i) an orthorhombic

supercell with two GBs and two grains (bulk regions) with $L_1 \times L_2 \times L_3$ dimensions, where L_1 is perpendicular to the GB plane and L_2, L_3 are in the GB plane; (ii) the corresponding bulk supercell without GBs with the same $L_2 \times L_3$ dimensions and approximately the same number of atoms. To eliminate Pulay stresses caused by the incompleteness of the plane wave basis set with respect to volume changes [24] the hcp lattice constants were determined independently for each bulk supercell using a manual two-dimensional polynomial fitting of 16 cells (four different a and c lattice constants within $\pm 4\%$ deformation region). The obtained equilibrium lattice constants were used to construct cells with GBs. The equilibrium excess volume of a GB was determined by fitting excess volumes of several cells with different expansions normal to the interface plane ranging from -0.3 to $+0.5$ Å (different L_1), while the values of L_2 and L_3 were fixed.

To study the interactions of impurities with a GB, we placed impurity atoms at different positions in the optimized supercell and relaxed the cell by adjusting all internal coordinates and the size of the supercell in the direction perpendicular to the GB plane. In all cases the $L_2 \times L_3$ dimensions of the cells with GBs were adopted to the $L_2 \times L_3$ dimensions of the corresponding bulk supercells with impurities. By this we take into account that the solid solution of impurities has slightly different lattice constants than that in the case of pure α -Ti. To study segregation of C and O, and C–O co-segregation, all interaction energies were calculated using supercells with two impurity atoms: 1. C–O pair in the GB region; 2. C–O pair in the bulk region; 3. one impurity atom in the GB region and one impurity atom in the bulk region; 4. a C atom in the first bulk region, an O atom in the second bulk region. To obtain the equilibrium excess segregation energy and volume of impurities we considered several expansions of the supercell normal to the interface plane, and as in the case of pure boundaries ranging from -0.3 to $+0.5$ Å.

The computational setup, including errors due to the periodic boundary conditions has been estimated to provide the following precision:

- 20 mJ m^{−2} (1.25 meV Å^{−2}) for GB energies;
- 50 meV for segregation and interaction energies;
- 150 meV for co-segregation energies.

The numbers mainly result from a supercell sizes convergence and show the errors for most difficult situations. For a large number of the considered configurations the errors are smaller, which is described in detail in supplementary sections 3 and 4 (stacks.iop.org/JPhysCM/28/385001/mmedia).

3. Grain boundaries in α -Ti

3.1. Description of the chosen GB structures

The modeling of general type GBs requires the construction of supercells with a large number of atoms making them presently inaccessible by first-principles methods due to the limitation of computer resources. However, there is a specific subset of coincidence site lattice (CSL) boundaries with low Σ values, which are known as twin boundaries [25].

Table 1. Geometrical parameters of considered twin boundaries.

Twin	System	Rotation	Angle	Shift	Along
T1m	{10 $\bar{1}$ 2}<1011>	[1 $\bar{2}$ 10]	84.8°	—	—
T1g	{10 $\bar{1}$ 2}<1011>	[1 $\bar{2}$ 10]	84.8°	$\sqrt{3a^2 + c^2}/2$	[1011]
T2	{11 $\bar{2}$ 1}<1 $\bar{1}$ 26>	[1 $\bar{1}$ 00]	34.5°	$\sqrt{3}a/3$	[1 $\bar{1}$ 00]
C1	{11 $\bar{2}$ 2}<1 $\bar{1}$ 23>	[1 $\bar{1}$ 00]	64.6°	—	—

In Ti alloys the importance of the twinning process was repeatedly confirmed during conventional deformation [26–30] as well as during the creation of a nano-sized GB structure [31].

Several twin boundaries with different orientation relations are observed in Ti. The twins are divided into two groups depending on the type of deformation: tensile twins, which accommodate *c*-axis elongation, and compression twins, which accommodate *c*-axis contraction [32]. The geometric parameters of the considered twins are collected in table 1.

Two tensile twins, usually labeled as T1 and T2, are characterized by 11 coinciding lattice sites ($\Sigma 11$). It is known that T1 is one of the predominant twinning modes in α -Ti [26]. We considered two possible variations of this twin T1m and T1g, which are called mirror and glide structures. Both variants were studied earlier using an *ab initio* approach [33] and the mirror variant was additionally investigated with the help of embedded atom method (EAM) potentials and molecular dynamics simulations [34].

The T2 twin is less common than T1, but it is considered as a potential damage nucleation site in the material due to the large shear [30]. The twin was theoretically studied earlier [35, 36] and it was shown that after mirroring the whole closed-packed layer in one grain should be shifted along the [1 $\bar{1}$ 00] direction. Without such a shift the twin becomes unstable due to the small distances between atoms (~ 0.15 Å). A recent *ab initio* study of this twin was made in [36].

The compression twins C1 and C2 are known as CSL boundaries $\Sigma 7$ and $\Sigma 13$, respectively. Among these two compression twins C1 is more commonly observed. It has been found that after tensile deformation up to 20% of all high-angle boundaries in pure Ti are C1 [29]. We have chosen for our investigation only C1. The structure and energy of this twin in α -Ti was considered earlier in [37] using EAM potentials and molecular dynamics simulations.

Finally, in addition to highly symmetrical low energy twin boundaries we have considered a high-energy $\Sigma 7(12\bar{3}0)$ boundary (S7) with a misorientation of 21.8° around the [0001] axis and a disordered structure. The S7 boundary was investigated in a previous study [12]. To check the final atomic structure of this boundary we have constructed four cells with lateral shifts of 0, 5, 10, and 15% of the *c* lattice constant in [0001] direction followed by atomic relaxation.

The simulation cells and the relaxed atomic geometries for the mentioned boundaries are shown in figure 1. For all considered boundaries the final relaxed atomic structure obtained in this work coincides with that in the literature.

3.2. GB energies and excess volumes

The energy of a GB (γ) and its excess volume (*e*) are important characteristics, which depend on the geometrical orientation of the grains and the internal atomic structure of the boundary. While the knowledge of γ is required to estimate the influence of segregation on GB thermodynamic stability, the evaluation of the excess volume is highly desirable since it can markedly influence diffusion and GB segregation phenomena [38].

We note that the alternative concept of ‘GB width’ is widely used in the literature. While a GB excess volume is defined as the difference of volumes of samples with GB and without GB (per GB unit area), the width of a GB is less strictly defined and depends upon the chosen model for GB description.

The GB excess volumes and energies were calculated from five different uniaxial strains according to the following equations:

$$\gamma_i = [E_{GB}(n, L_1^i, L_2, L_3) - \frac{n}{m}E_{bulk}(m, L_1^b, L_2, L_3)]/S \quad (1)$$

$$e_i = [V_{GB}(n, L_1^i, L_2, L_3) - \frac{n}{m}V_{bulk}(m, L_1^b, L_2, L_3)]/S, \quad (2)$$

where $E_{GB}(n, L_1^i, L_2, L_3)$ and $V_{GB}(n, L_1^i, L_2, L_3)$ are the energy and the expanded volume of the orthogonal cell with two GBs and *n* Ti atoms, $E_{bulk}(m, L_1^b, L_2, L_3)$ and $V_{bulk}(m, L_1^b, L_2, L_3)$ are the energy and volume of the commensurate Ti hcp bulk supercell with the same L_2, L_3 lateral supercell sizes and *m* Ti atoms. The number of atoms in the bulk supercell (*m*) is chosen to be as close as possible to the number of Ti atoms (*n*) in the supercell with the GB. $S = 2L_2L_3$ is the total area of the GB interface. The equilibrium value of the GB energy and the corresponding excess volume are determined by straining the supercell along L_1^i , which is perpendicular to the GB plane. The considered strains cover an interval of 1 Å.

The achieved values provided in table 2 indicate that the correlation between the GB energy and excess volume is not obvious. On the one hand, the twin boundaries with ordered structures such as T1m, T1g and T2 have comparable negative excess volumes and relatively low GB energies, while the ordered twin C1 with slightly higher γ has a relatively large positive excess volume. On the other hand, despite the much larger GB energy, the unordered S7 boundary is characterized by an almost vanishing excess volume.

It is quite unusual that T1m, T1g and T2 have negative excess volumes. We found that without atomic relaxation the minimum of the GB energy always corresponds to a positive expansion. However, after relaxation, the atomic configuration with minimum energy has a negative expansion, which means that the volume per Ti atom in the structure with a GB is smaller than that in ideal bulk Ti. The negative excess volume can be a result of a finite cell size due to the constrained lateral dimensions (L_2 and L_3) and corresponding lateral stresses acting on the whole supercell. The stresses should vanish with the increase of the grain size normal to the GB plane. To check the influence of supercell size on excess volume we have increased L_1 from 27 to 41 Å on the example of T1m. Surprisingly, the obtained excess volume for the larger cell

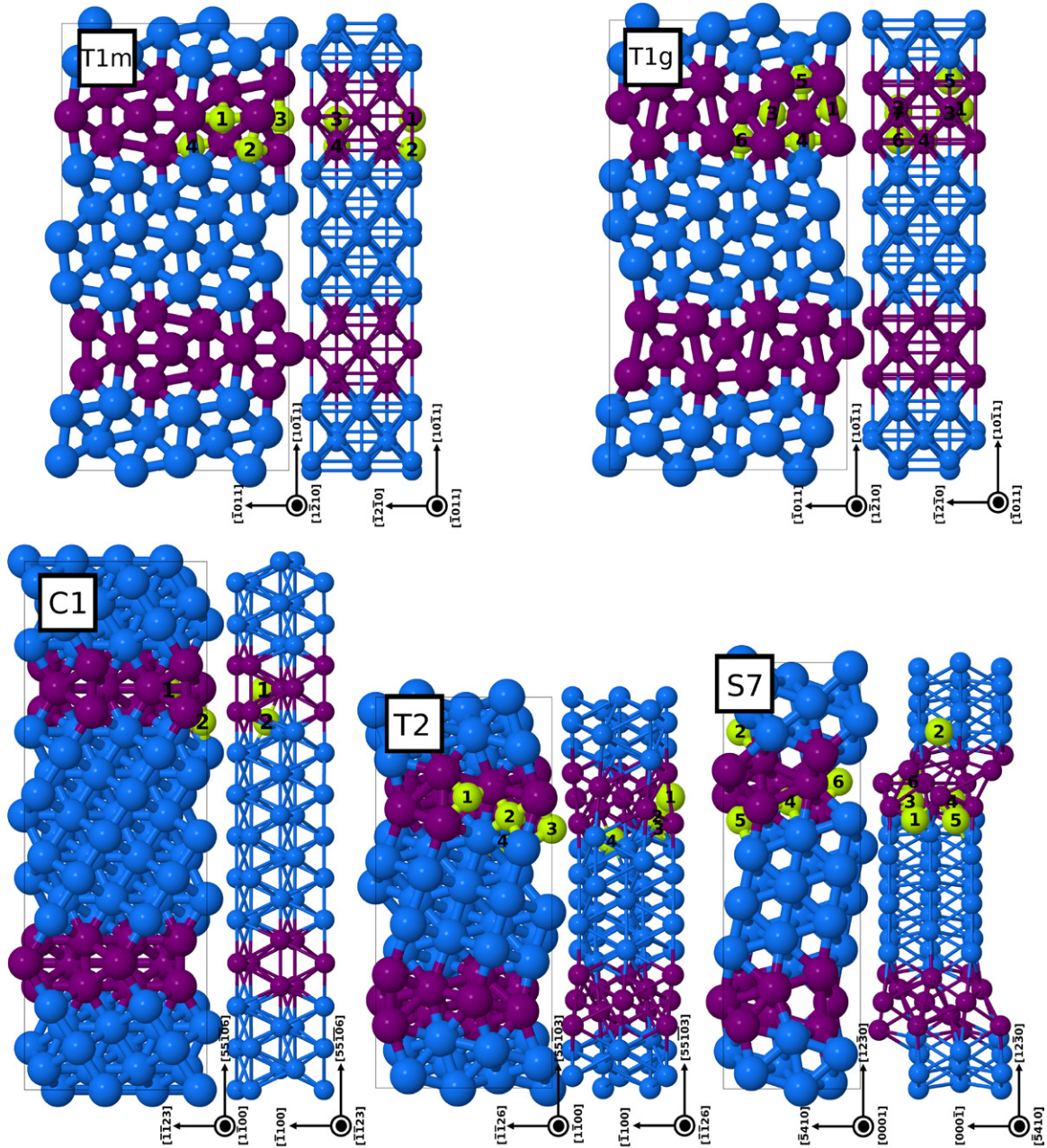


Figure 1. Structure of the supercells T1m, T1g, C1, T2 and S7 with corresponding GBs. Two views for each cell are shown. The atoms adjacent to the boundary atoms are distinguished with purple color. The considered positions for segregation are marked with numbered atoms.

Table 2. GB energy, γ (mJ m^{-2}), and excess volume, e (\AA), in comparison to literature data for T1, T2, C1 and four S7 boundaries with different lateral shifts, shown in parenthesis.

GB	C1	T1m	T1g	T2	S7	S7 (5%)	S7 (10%)	S7 (15%)
γ our	395	346	354	286	1084	1088	729	728
γ	521 ^d	307 ^a ; 242 ^b	304 ^a	235 ^c	—	—	—	—
e	0.210	−0.056	−0.054	−0.046	0.181	0.180	0.009	0.009

^a Norm-conserving LDA pseudopotentials [33].

^b EAM [34].

^c VASP PAW GGA with 4 valence electrons [36].

^d EAM [37].

Note: The mirror and glide versions of T1 are marked by m and g letters, respectively.

is still negative and even slightly smaller. Such behavior supports an assumption that the negative excess volume is an intrinsic property of T1m, which can be explained through the instability of α -Ti at 0 K. It is known, that at 0 K the most stable phase is ω -Ti, a hexagonal phase with $c/a < 1$, in which the volume per Ti atom is smaller by 0.2–0.3 Å³ than that in α -Ti [39]. Therefore, the transformation of seven atoms to the ω phase is sufficient to obtain a negative excess volume of −0.05 Å³ in the case of the T1m supercell. On the other hand, up to 12 atoms in the GB region can be considered as being part of the symmetrical GB phase having intermediate atomic volume between that for ω -Ti and α -Ti. Earlier, the transformation of GB region into ω -Ti was observed with the help of DFT [12], but still more careful examinations should be carried out.

4. C and O in bulk α -Ti

The segregation energies calculated using supercells can be affected by the interaction between the impurity and its periodic images. Therefore, the interaction between atoms should be carefully checked in the bulk region by calculating solution enthalpies and volumes for supercells of different sizes.

Both C and O are placed in octahedral voids of α -Ti, which is in agreement with experiment [40]. To calculate the solution enthalpy of C we use as a reference the energy of graphite. Since the GGA PBE functional overestimates the graphite lattice constants, we used experimental values for $a = 2.459$ Å and $c = 6.672$ Å determined at 4.2 K [41], with which graphite is still predicted as a groundstate structure and by 115 meV/atom lower than diamond. The solution enthalpy of O is calculated relative to the O₂ molecule. The obtained length of the chemical bond in the molecule of 1.23 Å is slightly larger than the experimental value of 1.21 Å [42].

The solution enthalpy (E_{sol}) and excess volume (ΔV) are calculated as follows:

$$E_{\text{sol}} = E(\text{Ti}_n\text{X}_1) - E(\text{Ti}_n) - E(\text{X}) \quad (3)$$

$$\Delta V = V(\text{Ti}_n\text{X}_1) - V(\text{Ti}_n) \quad (4)$$

where $X = \text{C}, \text{O}$. The expressions $E(\text{Ti}_n\text{X}_1)$ and $V(\text{Ti}_n\text{X}_1)$ are the energy and volume of the bulk supercell with n Ti atoms and one impurity atom, $E(\text{Ti}_n)$ and $V(\text{Ti}_n)$ are the energy and volume of the corresponding pure cells and $E(\text{X})$ is the reference energy. To study the influence of cell sizes on the solution enthalpy in α -Ti we have used four hexagonal-shaped supercells (called HCP) of different sizes and three almost orthogonal supercells which correspond to the considered supercells with T1, T2 and C1. The largest considered supercell Ti₂₀₀ (HCP) contains up to 14 coordination shells around the impurity atom.

The sizes of the considered cells, solution enthalpies and excess volumes are provided in table 3 for C and O. The obtained solution enthalpy of O in α -Ti with respect to the O₂ molecule (−5.6 eV/atom) is in agreement with experimental data (from −5.77 to −6.5 eV/atom [43, 44]) and with earlier VASP calculations by Boureau *et al* (−5.75 eV/atom) [45].

Table 3. Solution enthalpy E_{sol} (eV/atom), and absolute change of volume ΔV depending on the sizes L_1 , L_2 and L_3 (Å) of the simulation cell.

Cell	E_{sol}	ΔV	L_1	L_2	L_3
Ti ₈ C (HCP)	−1.557	7.2	5.94	5.94	4.79
Ti ₃₆ C (HCP)	−1.629	6.9	8.83	8.83	9.36
Ti ₉₆ C (HCP)	−1.619	7.0	11.75	11.75	14.00
Ti ₂₀₀ C (HCP)	−1.587	6.9	14.70	14.70	18.61
Ti ₄₈ C (T1)	−1.561	7.0	20.73	6.91	5.89
Ti ₄₄ C (T2)	−1.596	7.0	15.44	9.79	5.10
Ti ₅₆ C (C1)	−1.578	6.8	34.84	5.52	5.09
Ti ₈ O (HCP)	−5.688	3.6	5.89	5.89	4.74
Ti ₃₆ O (HCP)	−5.610	4.0	8.82	8.82	9.34
Ti ₉₆ O (HCP)	−5.594	4.2	11.74	11.74	13.99
Ti ₂₀₀ O (HCP)	−5.592	3.7	14.69	14.69	18.60
Ti ₄₈ O (T1)	−5.587	3.8	20.70	6.90	5.88
Ti ₄₄ O (T2)	−5.630	4.0	15.42	9.77	5.09
Ti ₅₆ O (C1)	−5.664	3.8	34.80	5.51	5.09

For carbon (−1.62 eV) we also have a good agreement of solution enthalpies with the PAW GGA result of Hennig *et al* [46] (−1.58 eV). The solution enthalpies for C and O show a different behavior in Ti₈ (HCP) and Ti₃₆ (HCP) cells. For C the solution enthalpy in Ti₃₆ (HCP) is smaller than in Ti₈ (HCP) cell by 72 meV. In contrast to this, O has a higher solution enthalpy in Ti₃₆ (HCP) than in Ti₈O by 78 meV. The discussion of the influence of the supercell size on the solution enthalpy is provided in supplementary section 1. In summary, we obtained a good convergence with respect to the cell sizes. By using a Ti₉₆ (HCP) supercell the solution enthalpies of C and O are converged within 30 meV and 2 meV, respectively.

The values of the excess volumes ΔV for C and O are similar for all cells and lie around 7 Å³ and 4 Å³, respectively. They are in qualitative agreement with the experimental values of excess volume of hydrogen in fcc metals (~3 Å³) [47]. The obtained scatter of 0.1–0.5 Å³ of excess volumes even for largest supercells is due to the strong influence of small errors in determining lattice constants (0.001 Å). The positive values can be understood within a hard-spheres model: assuming the metallic radius of Ti to be 1.44 Å, the radius of the hard sphere which can be inserted in the octahedral void is 0.62 Å. At the same time the covalent radius of C is 0.69–0.76 Å. As a result, the insertion of an impurity slightly increases the distances between neighboring Ti atoms from 2.88 and 2.93 to 2.94 and 2.97 Å, enlarging the volume of the occupied octahedron by approx. 0.5 Å³. However, the volumes of the neighboring octahedra and tetrahedra are also increased by comparable values. Hence, only a small part of the excess volume is directly related to the occupied void, while the rest is distributed among the supercell due to the increased bond lengths.

A more precise estimate of the excess volume related to the filled octahedral void is obtained by a Voronoi construction [48, 49]. Accordingly, the volume of the ideal octahedral void in pure Ti is 8.7 Å³, while after adding C and atomic relaxation, it increases up to 9.05–9.24 Å³, confirming that

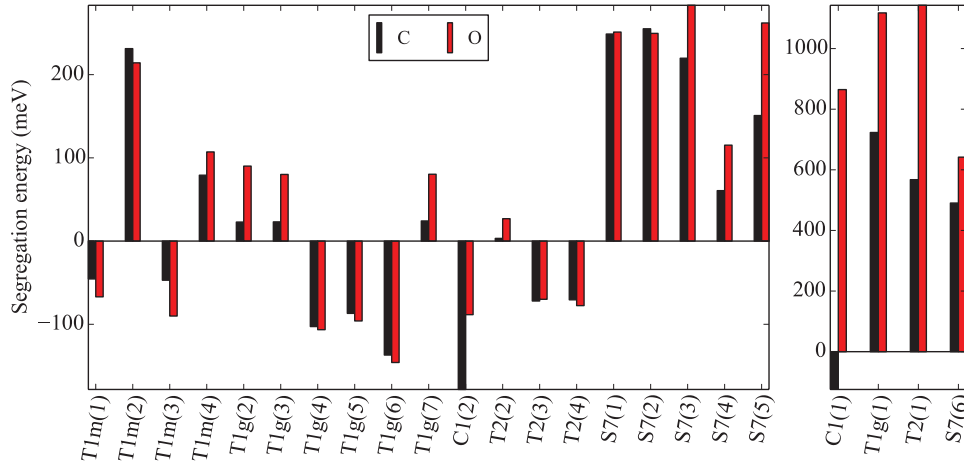


Figure 2. Segregation energies of C and O calculated for all considered segregation configurations using equation (5). Pay attention to the different energy scale of the right pane.

only $\sim 0.4 \text{ \AA}^3$ of the excess volume is associated explicitly with the swelling of the filled void.

A similar situation is observed for O. The covalent radius of O (0.66 \AA) is slightly smaller than for C and matches with the smaller excess volume of 4 \AA^3 . However, the values of the Voronoi volume of the voids filled with O are almost the same as for the voids with C. Hence, the larger excess volume in the case of C should be connected to the larger neighboring voids.

To clarify the influence of the void size on the solution enthalpy of the impurity, we have calculated E_{sol} (equation (3)) for several uniformly contracted and expanded hexagonal supercells. We obtained that C and O prefer octahedral voids that have due to expansion a larger volume. The details are provided in supplementary section 2. The enlargement of the interstitial voids is common at GBs, and the impact of this mechanism on GB segregation will be studied in the following.

5. Energies of independent segregation of C and O in α -Ti

To study the interaction of impurities with the considered GBs we have chosen 23 inequivalent segregation voids (7 for T1g, 4 for T1m, 4 for T2, 2 for C1, and 6 for S7). The positions of the sites are indicated by numbers in figure 1. The obtained Gibbs excesses at T1, T2, C1 and S7 are 0.025, 0.02, 0.035 and 0.027 atom \AA^{-2} , respectively. Since the solution enthalpies of C and O in bulk Ti are much higher for tetrahedral voids (by 2.1 eV for C and 1.2 eV for O [46]) as well as for substitutional positions (by $\sim 3 \text{ eV}$ [50]), we consider segregation only in various distorted octahedral voids and larger voids with more complex coordination.

The key segregation characteristics such as segregation energies and volumes were calculated for five different GB expansions (e_i) according to the following equations:

$$E_{\text{seg}} = E_{\text{GB}}(\text{X in GB}) - E_{\text{GB}}(\text{X in gr}) \quad (5)$$

$$V_{\text{seg}} = V_{\text{GB}}(\text{X in GB}) - V_{\text{GB}}(\text{X in gr}), \quad (6)$$

where E_{GB} and V_{GB} are equilibrium energy and volume of supercells with two GBs and two grains. The impurity atom X is situated either in the GB interior (X in GB) or inside the grain (X in gr). The equilibrium values of E_{GB} and V_{GB} correspond to zero stress along L_1 and minima of energies; they are found by a quadratic fit of $E_{\text{GB}}^i(\text{X in GB})$ and $E_{\text{GB}}^i(\text{X in gr})$ with respect to corresponding volumes.

A negative value of E_{seg} means that it is more favorable for the impurity atoms to be in the GB region than in the grain interior. The segregation energies are visualized in figure 2, while their values along with volumes and other geometry data are summarized in the supplementary table S5. First of all, it should be noted that for the majority of the configurations the qualitative behavior of C and O is quite similar. Therefore, further in the text, if the type of impurity is not specifically mentioned, the provided statement is valid both for C and O.

It is seen from figure 2 that at the high-energy GB S7 with its disordered structure the segregation is always unfavorable regardless of the void position. In contrast to this, more symmetric low-energy twin boundaries have a number of positions, which are characterized by negative E_{seg} values. However, the thermodynamic driving force for segregation remains low (-138 meV and -155 meV for C in T1g(6) and C1(2), respectively) in comparison to segregation energies in other materials (e.g. -830 to -2200 meV for C in α -Fe [51]). The twin boundaries also have several voids that are completely unfavorable for segregation. Moving a C atom from the bulk region to the T1g(1) or T2(1) voids, the total energy of the system increases by more than 500 meV.

It is quite important that there are noticeable differences in segregation energies for T1m and T1g, though they have equivalent geometrical orientations and similar GB energies (the difference is 7 mJ m^{-2}). For C at T1m the most favorable void is T1m(1) with a segregation energy of -50 meV , while for the T1g the most favorable void T1g(6) has a segregation energy of -138 meV . The strong dependence of segregation energies on the particular atomic structure indicates that the knowledge of five geometrical parameters for the GBs,

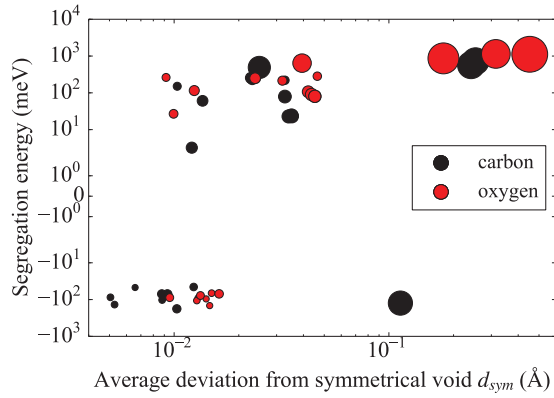


Figure 3. The dependence of segregation energy, E_{seg} , on the average deviation, $d_{\text{dev}}^{\text{end}}$, calculated with equation (7). The sizes of the points are proportional to the Voronoi volume of the voids $V_{\text{vor}}^{\text{end}}$. The configurations with negative segregation energies and small deviations are C1(2), T1g(6), T1g(4), T1g(5), T2(3), T2(4), T1m(3), and T1m(1).

usually determined by the present experimental techniques, is insufficient for a systematic study of segregations in experimental works.

The influence of the grain boundary expansion (ϵ) from -0.3 to $+0.5$ Å on the segregation energies is for the majority of configurations at T1, T2 and S7 boundaries in the order of $\pm 25\%$ around its equilibrium values (with maximum deviations up to $\pm 90\%$ for selected configurations). For the C1 this influence is more pronounced, for example E_{seg} for C1(1) C changes from -230 meV to $+167$ meV with an equilibrium value near 0 meV. The effect of volume relaxation on segregation energies in comparison to the original excess volume of a pure grain boundary is rather small and does not exceed $\pm 20\%$, except for the case of C1(1) C, where it changes from -72 to $+1$ meV.

5.1. Correlation between segregation energies and atomic geometry

In order to understand the different segregation energies, we have studied the influence of the atomic geometry. The relation between the segregation volumes V_{seg} and segregation energies E_{seg} did not provide the intended insights, since the trends strongly depend on the type of twin boundary. For T1g negative segregation energies are combined with positive excess volumes, while for C1 and T2 both segregation volumes and energies have negative values. For T1m both combinations of energy and volume signs are found.

A further challenge of this analysis is that the values of V_{seg} are quite sensitive to the impurity-image interaction. By performing systematic tests we realized that it is more reliable to use Voronoi volumes of the voids as well as their coordination and geometry for the analysis. According to the coordination and geometry all considered voids can be divided into three groups: voids with octahedral symmetry with low distortions, highly distorted octahedral voids, and voids with a complex

structure that have seven or eight neighboring Ti atoms (such as C1(1), T1g(1), and T2(1)). To quantify the deviation of a void from its fully symmetrical version (where all distances between the center of the void and its nodes are the same) the following parameter will be used:

$$d_{\text{dev}} = \frac{1}{N} \sum_i |d_i - d_{\text{av}}| \quad \text{with} \quad (7)$$

$$d_{\text{av}} = \frac{1}{N} \sum_i d_i \quad (8)$$

where d_i is the distance between the impurity and the Ti atom i of the void, N ($=6, 7$ or 8) is the number of Ti atoms around the impurity in the void. For octahedral voids $N = 6$. For the voids C1(1), T2(1), and T1g(1) $N = 7$ or 8 .

The values of d_{dev} were calculated before ($d_{\text{dev}}^{\text{init}}$) and after ($d_{\text{dev}}^{\text{end}}$) the relaxation of the atomic structure. The dependence of E_{seg} on $d_{\text{dev}}^{\text{end}}$ (see figure 3) shows that octahedral voids with larger deviations and larger Voronoi volumes $V_{\text{vor}}^{\text{end}}$ are less favorable for segregation. The latter seems to be inconsistent with the result obtained in section 4, where we observed for the bulk α -Ti lattice that C and O atoms prefer the voids with larger Voronoi volumes. However, for the considered voids at GBs a larger Voronoi volume always corresponds to a void with lower symmetry. We can therefore conclude that the influence of local atomic coordination on the segregation energy is more pronounced than that of the Voronoi volume.

The predominant relevance of the local coordination is similar to the behavior of hydrogen in iron that was found by us earlier [49]. The preference of symmetric voids by C and O in Ti, however, is opposite to the trend observed there. More specifically, hydrogen atoms in distorted interstitial voids have much lower segregation energies than those for more symmetrical voids.

The discovered influence of the void coordination and structure on segregation energies allows us to establish a correlation between the E_{seg} for C and O and the GB energy in Ti. The GB with a more disordered structure is characterized by a higher GB energy and has more unsymmetrical voids with larger positive E_{seg} values (S7). In contrast to that a highly symmetrical boundary has lower GB energies and smaller negative E_{seg} values (T1, T2 and C1).

The preference of the octahedral voids with lower d_{dev} values also implies that the relaxation of the atoms next to an interstitial atom increases the symmetry of the strongly distorted voids. For the majority of cases the value $d_{\text{dev}}^{\text{end}}$ is smaller than that of $d_{\text{dev}}^{\text{init}}$. However, this symmetrization is accompanied with an increase of the GB energy due to the additional mechanical deformation of its equilibrium structure. To check this we separated segregation energies into a chemical and a mechanical (strain) contribution, as described in our previous work [12]:

$$E_{\text{seg}}^m = E_{\text{GB}}(\text{Vac in GB}) - E_{\text{GB}}(\text{Vac in gr}), \quad (9)$$

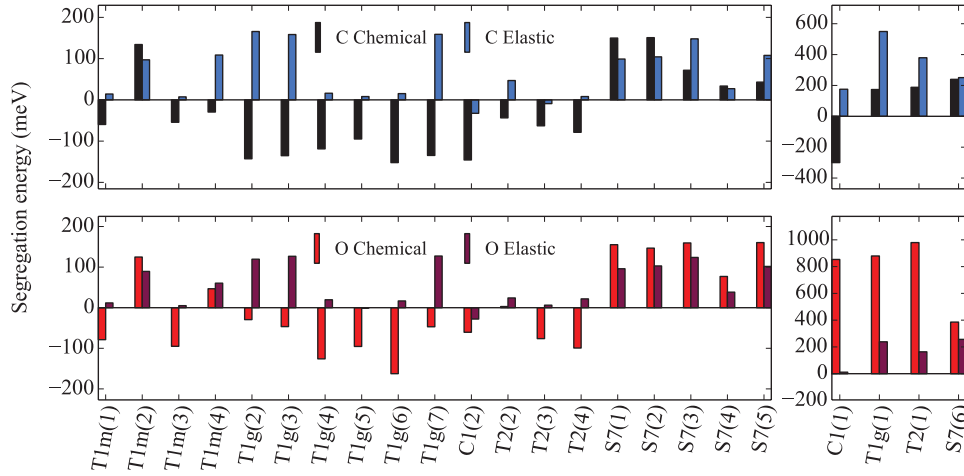


Figure 4. Chemical and mechanical contributions to segregation energies for C and O for all considered segregation configurations. The contributions are calculated in analogy to that provided by equation (9). Note the different energy scale of the right panel.

$$E_{\text{seg}}^{\text{ch}} = E_{\text{seg}} - E_{\text{seg}}^m, \quad (10)$$

where $E_{\text{GB}}(\text{Vac in GB})$ and $E_{\text{GB}}(\text{Vac in gr})$ are the total energies of the supercells, obtained by removing the interstitial impurity atoms and fixing the Ti atoms. The corresponding values are visualized in figure 4. The idea of splitting the energies into mechanical and chemical contributions has been used in several succeeding works [52–54], mainly in the context of binding energies and can be readily applied to segregation energies.

It can be seen that for highly symmetrical voids such as T1m(1, 3), T1g(4, 5, 6), and T2(3, 4) the mechanical contribution to the segregation energy is very small (≤ 20 meV). As a result, owing to the negative chemical contribution the E_{seg} is also negative. For the less symmetrical voids 2, 3 and 7 at T1g the mechanical contribution is much larger and E_{seg} is positive—despite the negative chemical contribution. Finally, for the remaining completely unsymmetrical voids the mechanical contributions have the largest values. If the distortions at the GB are too large, the optimization of the local coordination is less likely to occur. Therefore, for such voids the chemical contributions are also positive, resulting in very large positive values of E_{seg} .

The C1(2) void is distinctive for its negative mechanical contribution (−33 meV), which is attributed to the smaller relaxation effects next to the impurity at the GB as compared to those in the grain interior.

As was mentioned earlier, for the majority of the considered voids C and O atoms show a very similar behavior with only moderate quantitative variations. However, for several voids that are 7 or 8 fold coordinated (C1(1), T2(1), and T1g(1)) much stronger differences are observed. For example, the mechanical contributions are much larger in the case of O. Since O atoms have a lower flexibility to form various hybridization shapes, there is a stronger driving force to rearrange the surrounding Ti atoms such that the interstitial has only six neighbors with octahedral symmetry. As a result the initial equilibrium structure of the boundary is significantly distorted. In turn, a C atom can

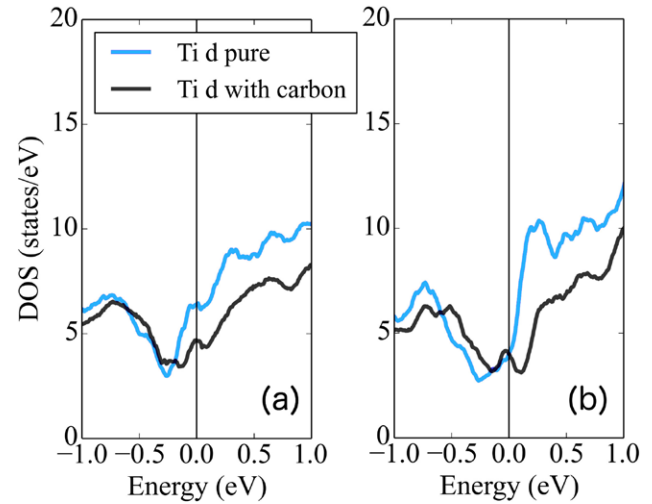


Figure 5. The partial density of states of d -orbitals summed for the six Ti atoms adjacent to the C1(2) segregation void (a) and for the six Ti atoms next to a bulk void in the C1 cell (b). The Fermi level is at 0 eV. It is seen that the reduction of the PDOS at the Fermi level due to the insertion of a C atom is much larger in the case of a void at the GB.

form more bonds and therefore influences the geometry of the void to a smaller extent.

5.2. Correlation between segregation energies and electronic structure

For a deeper understanding of the obtained trends in the segregation energies we calculated partial densities of electronic states (PDOS).

We find a strong correlation between the chemical contribution of the segregation energies and the reduction of the d -PDOS at the Fermi level for the majority of voids (C1(1), C1(2), T1g(6), T2(4) are most pronounced). An example of the PDOS for the C1(2) segregation void in comparison to octahedral void in bulk is shown in figure 5, where different d -PDOS reductions are clearly seen. Despite the higher values of the d -PDOS at the GB than in the grain interior,

a segregation of an impurity is favorable due to the more effective optimization of the electronic structure at the GB. However, in the case of octahedral voids, there is one important condition to make such a transfer favorable: The voids at the GB should not be too heavily deformed. This is because the *s-p-d* hybrid orbital formed by C or O in Ti has itself an octahedral symmetry. Hence, the impurity tries to symmetrize a deformed void, which in turn is not required for the GB with optimal geometrical structure. Examples of such unfavorable configurations are T1g(1,3,2,7), S7(1,2,6), and T1m(2, 4).

6. The interaction between C–C, O–O, and C–O in bulk Ti

6.1. Impurity pairs in hexagonal Ti

Before going to the co-segregation the study of C–C, O–O, and C–O pairs for 15 configurations with different orientations and lengths was performed in the Ti_{96} (HCP) cell. Based on the experiences with single impurity atoms (table 3), the volume was expanded such that the final external pressure for the cell with two impurity atoms is close to zero. The chemical trends, however, have been investigated for a fixed shape and volume of the supercell, while all atomic positions were relaxed.

The interaction energies of X–Y pairs are defined with respect to the pair with the maximum distance of 9.14 Å (№15), for which the mutual influence of impurity atoms is small and will be neglected:

$$E_{\text{pair,bulk}}(\text{X} - \text{Y}) = E(\text{X} - \text{Y})_i - E(\text{X} - \text{Y})_{15}. \quad (11)$$

Here, $E(\text{X} - \text{Y})_i$ is the total energy of the Ti_{96}XY supercell (configuration *i*). To separate the specific features of the C–O interactions from the monoatomic interactions we compare $E_{\text{pair,bulk}}(\text{C} - \text{O})$ with the the average value of $\Delta E_{\text{av}} = [E_{\text{pair,bulk}}(\text{C} - \text{C}) + E_{\text{pair,bulk}}(\text{O} - \text{O})]/2$.

The dependence of the interaction energies $E_{\text{pair,bulk}}(\text{X} - \text{Y})$ on the interatomic distance is shown in figure 6. Our results for $E_{\text{pair,bulk}}(\text{O} - \text{O})$ can be compared with earlier first-principles calculations [45] that obtained for positions (№1–3) the values 510, 80 and 40 meV, respectively. The deviation of their third value is due to the fact that a too small supercell (Ti_{48}O_2) was used by the authors [45].

Analyzing figure 6 two regions can be distinguished, due to their different nature of the interatomic interaction. The configurations №1–4 with interatomic distances smaller than 4.7 Å show quantitatively deviating pair interaction energies for the C–C, O–O, and C–O pairs. It is evident that for these distances the energy $E_{\text{pair,bulk}}(\text{X} - \text{Y})$ has a strong chemical contribution, which explains the differences between O and C. The configuration №2 shows even a different sign of energies for the C–C (–19 meV) as compared to the O–O pair (80 meV). The average value of these two numbers is 30 meV, whereas the interaction between C and O (–24 meV) is not only smaller than this average, but also smaller than both individual terms. The third configuration is also interesting: $E_{\text{pair,bulk}}(\text{X} - \text{Y})$ for C–C as well as O–O is about 5 meV, while for the C–O pair the value is –24 meV. These effects indicate the existence of particular electronic features that are specific for C–O bonds.

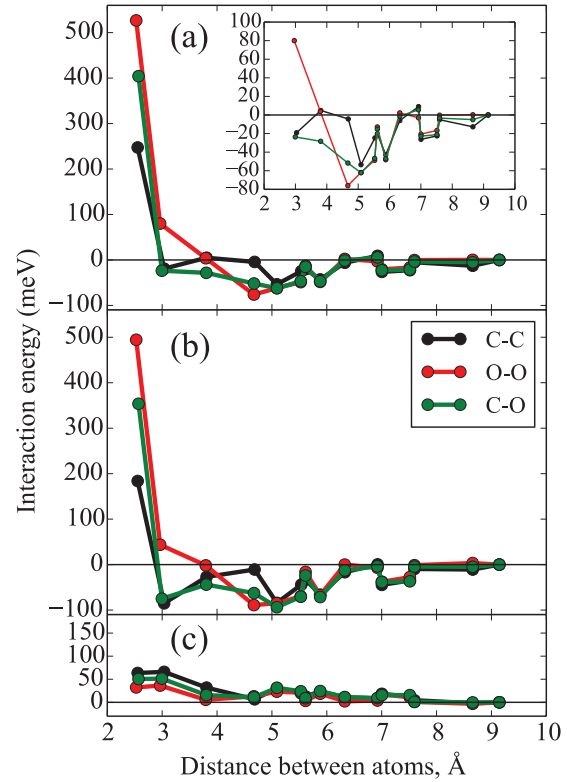


Figure 6. The dependence of the interaction energies $E_{\text{pair,bulk}}(\text{X} - \text{Y})$ for C–C, O–O, and C–O pairs on the atomic distance in the Ti_{96} (HCP) cell (a), the corresponding dependencies of the chemical contribution (b), and mechanical dependencies (c). The inset details the interaction energies starting from configuration №2. The interaction is attractive if the values are negative.

Beginning from configuration №5 (5.09 Å) $E_{\text{pair,bulk}}(\text{X} - \text{Y})$ is almost the same for the C–C, O–O, and C–O pairs, at first sight indicating that these interactions are of purely elastic nature. In order to check this in more details we have separated $E_{\text{pair,bulk}}(\text{X} - \text{Y})$ into chemical and mechanical contributions as described in section 5. The contributions are shown in figures 6 (parts (b) and (c)). It turns out that the mechanical contributions, which are related to the strain of the Ti lattice, are comparatively small. Actually they are of the same order for all considered configurations and are decreasing with the distance between impurity atoms. For the C–C pair the elastic interaction is slightly stronger than for the O–O pair, which is consistent with the larger excess volume of C in Ti (see table 3). The main contribution to $E_{\text{pair,bulk}}(\text{X} - \text{Y})$ comes even for distances larger than 7 Å from the chemical contribution, which can indicate host-induced interactions between impurities.

It can be concluded that in comparison to C–C or O–O, the interaction between C and O has its own features (e.g. an additional attraction in the case of the third configuration), due to chemical effects. Owing to the small magnitude, it is difficult to explain these effects in terms of the electronic structure changes. However, the chemical effects may be more pronounced for the case of less symmetrical structures such as GBs, making the study of C–O co-segregation relevant. This goes along with the open question whether co-segregation or just competitive segregation of C and O was observed experimentally next to Ti GBs [9].

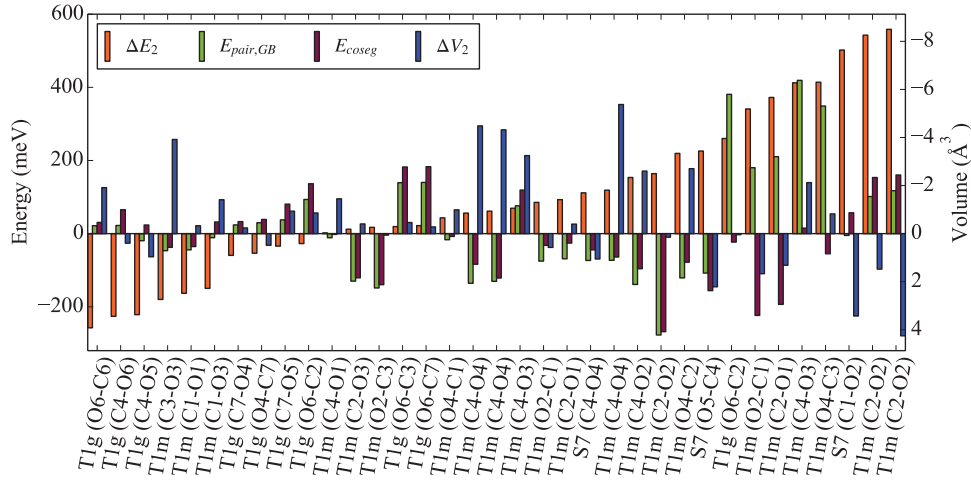


Figure 7. Energies and volumes of C–O interaction at T1g, T1m, and S7 calculated using equations (12)–(15). The ordering is made according to the increase of ΔE_2 .

7. C–O co-segregation at GBs in α -Ti

In order to investigate the co-segregation of C and O atoms, all C–O configurations for the segregation voids up to a certain distance next to the GBs investigated in section 5 have been taken into account. More specifically, a maximum distance between C and O of 4.8 Å and a maximum distance of C and O from the GB plane of 3 Å have been considered. For T1g and S7 only the most relevant C–O configurations defined by the smallest independent segregation energies (see section 5) have been accounted.

In the same spirit as for the independent segregation energies (equations (5) and (6)) the mutual interaction energies of C–O pairs with GBs were calculated as:

$$\Delta E_2 = E_{\text{GB}}(\text{C} - \text{O in GB}) - E_{\text{GB}}(\text{C}, \text{O in gr}) \quad (12)$$

$$\Delta V_2 = V_{\text{GB}}(\text{C} - \text{O in GB}) - V_{\text{GB}}(\text{C}, \text{O in gr}), \quad (13)$$

where $E_{\text{GB}}(\text{C} - \text{O in GB})$ and $V_{\text{GB}}(\text{C} - \text{O in GB})$ are the energy and volume of a supercell in which a C–O pair is situated at a GB. The label ‘gr’ indicates that both impurity atoms are situated in the grain interior, one atom in each of the grains, while the GBs are empty. A negative energy is required, to ensure a simultaneous segregation of C and O. Indeed, it is seen from figure 7 that a number of C–O pairs at T1m and T1g have negative ΔE_2 energies with minimum values of ~ -260 meV.

It is important to determine whether the interaction between C and O atoms at GBs is attractive or repulsive and how it differs from the interaction of C and O in the bulk. For this purposes we introduce two additional energy characteristics:

$$E_{\text{pair,GB}} = \Delta E_2 - E_{\text{seg}}(\text{C}) - E_{\text{seg}}(\text{O}) \quad (14)$$

$$E_{\text{coseg}} = E_{\text{pair,GB}} - E_{\text{pair,bulk}}. \quad (15)$$

Here, $E_{\text{pair,GB}}$ is the gain of energy due to the joining of independently segregated atoms, while $E_{\text{pair,bulk}}$ is the gain of energy due the formation of C–O pair in the bulk region of

supercell as described in section 6 (for details see supplementary section 4). E_{coseg} shows to what extent the interaction between impurities at the GB differs from the interaction in the bulk (by comparing pairs with similar separations). Negative values of E_{coseg} means a more favorable formation of C–O pairs in the GB region than in the bulk region. The values of $E_{\text{pair,GB}}$, E_{coseg} are also visualized in figure 7 and in supplementary figure S2.

Focusing first on T1m, one realizes that for the first three C–O configurations with negative ΔE_2 , the co-segregation energies E_{coseg} fall into an interval of ± 38 meV. Such small numbers imply that the C–O interaction in T1m is similar to that in the bulk region. Therefore, the presence of one element in the GB does not support the segregation of the other. However, for several configurations with positive ΔE_2 , the co-segregation energies are negative (for T1m (C2-O2) up to -271 meV). This means that a pair formation in the GB is highly favorable, but is hardly relevant in equilibrium since the segregation of the individual impurities is suppressed. Still in non-equilibrium conditions such as severe plastic deformation and radiation induced segregation, additional energy gain at GBs can be important. A similar situation (negative E_{coseg} together with unfavorable independent segregation) is observed for T1g and T2: whenever the configurations have negative ΔE_2 values, the E_{coseg} is slightly positive (20–60 meV for T1g, and 10–100 meV for T2).

The C1 (C01) and S7 (C6-O4) are examples of configurations in which C and O atoms are both situated in one void. The huge positive values of ΔE_2 of ~ 2 eV show that such configurations are highly unfavorable.

A connection of the change of volume ΔV_2 (also provided in figure 7) with ΔE_2 is not straightforward and depends on the type of boundary. For the C1 negative values of formation volumes are caused by a significant reduction of the GB void volume after impurity addition.

Based on the large number of considered C–O configurations and the large number of GBs we conclude that thermodynamically stable co-segregation (both ΔE_2 and E_{coseg} negative) is unlikely in α -Ti.

8. Conclusions

We have used first-principles methods to study the solution and GB segregation of C and O atoms in α -Ti. Both interstitial elements are considered independently as well as in combination. In this way we improve the understanding to which degree these impurities enhance the stability of five different GBs, including the most often experimentally observed twin boundaries.

Since segregation energies are given by energy differences, GB and bulk structures, as well as atomic configurations with and without impurities had to be considered. The energies of the five GBs without impurities cover a range of 290–400 mJ m⁻² for the highly symmetrical twin boundaries and 730 mJ m⁻² for the less symmetrical $\Sigma 7$ boundary. Some of the GBs have a negative excess volume.

Since the reference point for the segregation process is the chemical potential in the bulk of the material, the calculated solution enthalpies and volumes of C and O in Ti have been compared for different concentration regimes. These impurity-containing bulk systems confirm the convergence of solution enthalpies for the used supercell sizes. The obtained positive solution volumes for C (7 Å³) and O (4 Å³) in octahedral interstitial voids indicates the possibility of grain boundary segregation. Moreover, we found that the solution is more favorable for larger void volumes, which were also found inside the optimized GBs.

Surprisingly, the calculation of C and O GB segregation energies for 23 different voids resolved that a larger volume of a void next to the boundary typically does not yield a gain in energy. Instead, we found that the symmetry of the voids is more important and determines whether a segregation is energetically attractive. As a result the symmetrical twin boundaries which incorporate symmetrical octahedral voids are favorable for segregation, while the less symmetrical $\Sigma 7$ boundary contains only unfavorable voids for segregation. Although a large amount of GBs and voids has been considered, the favorable voids are characterized by segregation energies between –50 and –160 meV. On the one hand, this narrow window of the energies allows to generalize the behavior of C and O for a wider range of ordered GBs. On the other hand, relatively low values of segregation energies imply only a weak enrichment of GBs in α -Ti. A key mechanism for segregation at twin boundaries in the case of symmetrical voids is the enhanced reduction of the Ti *d*-PDOS at the Fermi level when adding an impurity in comparison to that in the bulk crystal.

To determine whether a co-segregation of C and O explains the experiments on polycrystalline Ti [9], we compared the formation of C–O pairs in the bulk of Ti with the situation in the GBs. Already in the bulk we obtain that formation of C–O bonds for several cases have additional energy advantage in comparison to C–C and O–O bonds, which indicated for the possibility of C–O co-segregation at GBs.

However, the study of co-segregations for 75 different configurations at optimized GBs showed that almost no C–O co-segregation is possible under equilibrium conditions.

The simultaneous incorporation of both C and O atoms in one void is even more unfavorable and increases the energy of the system by 2 eV. Hence, most probably, in the previous experimental study, just the competitive GB segregation of C and O was observed.

Regarding a possible influence of C and O segregation at GBs on the thermal stability of nanostructured Ti, it could be concluded that these impurities are responsible for some stabilization of twin boundaries. However, a repelling of the impurities from general GBs and relatively weak enhancement of twin boundaries makes the segregation mechanism of C and O insufficient for the explanation of observed thermal stability in Ti. Hence, further studies of thermal stability mechanisms in nanostructured CP-Ti are required; these include influence of O solid solution on the mobility of GBs, and GB segregation of iron, accompanied with phase transformation of GB region to β -Ti.

Acknowledgments

The research that led to these results received funding from the German Academic Exchange Service DAAD and the Ministry of Education and Science of the Russian Federation through the Contract No. 3.1282.2014K

References

- [1] Greger M, Widomska M and Kander L 2010 *Achievements Mater. Manufact. Eng.* **40** 33–40
- [2] Handtrack D, Sauer C and Kieback B 2007 *J. Mater. Sci.* **43** 671
- [3] Stolyarov V V, Zhu Y T, Alexandrov I V, Lowe T C and Valiev R Z 2001 *Mater. Sci. Eng. A* **299** 59
- [4] Hoseini M, Hamid Pourian M, Bridier F, Vali H, Szpunar J A and Bocher P 2012 *Mater. Sci. Eng. A* **532** 58
- [5] Kolobov Y R, Lipnitskii A G, Ivanov M B, Nelasov I V and Manokhin S S 2011 *Russ. Phys. J.* **54** 918
- [6] Leyens C and Peters M (ed) 2003 *Titanium and Titanium Alloys Fundamentals and Applications* vol 1 (New York: Wiley) p 513
- [7] Ouchi C, Iizumi H and Mitao S 1998 *Mater. Sci. Eng. A* **243** 186
- [8] Koch C C, Scattergood R O, Saber M and Kotan H 2013 *J. Mater. Res.* **28** 1785
- [9] Semenova I, Salimgareeva G and Da Costa G 2010 *Adv. Eng. Mater.* **12** 803
- [10] Kwasniak P, Muzyk M, Garbacz H and Kurzydowski K 2013 *Mater. Lett.* **94** 92
- [11] Ghazisaeidi M and Trinkler D 2014 *Acta Mater.* **76** 82
- [12] Aksyonov D A, Lipnitskii A G and Kolobov Y R 2013 *Modelling Simul. Mater. Sci. Eng.* **21** 075009
- [13] Gil F and Planell J 2000 *Mater. Sci. Eng. A* **283** 17
- [14] Bozzolo N, Dewobroto N, Grosdidier T and Wagner F 2005 *Mater. Sci. Eng. A* **397** 346
- [15] Contieri R, Zanotello M and Caram R 2010 *Mater. Sci. Eng. A* **527** 3994
- [16] Solonina O P and Ulyakova N M 1974 *Met. Sci. Heat Treat.* **16** 310
- [17] Hohenberg P and Kohn W 1964 *Phys. Rev.* **136** B864
- [18] Kohn W and Sham L J 1965 *Phys. Rev.* **140** A1133
- [19] Perdew J, Burke K and Ernzerhof M 1996 *Phys. Rev. Lett.* **77** 3865

- [20] Blochl P E 1994 *Phys. Rev. B* **50** 17953
- [21] Kresse G and Furthmüller J 1996 *Comput. Mater. Sci.* **6** 15
- [22] Monkhorst H J and Pack J D 1976 *Phys. Rev. B* **13** 5188
- [23] Methfessel M and Paxton A T 1989 *Phys. Rev. B* **40** 3616
- [24] Francis G P and Payne M C 1990 *J. Phys.: Condens. Matter* **2** 4395
- [25] Zheng S, Beyerlein I J, Carpenter J S, Kang K, Wang J, Han W and Mara N A 2013 *Nat. Commun.* **4** 1696
- [26] Wang L, Yang Y, Eisenlohr P, Bieler T, Crimp M and Mason D 2009 *Metall. Mater. Trans. A* **41** 421
- [27] Wang L, Eisenlohr P, Yang Y, Bieler T and Crimp M 2010 *Scr. Mater.* **63** 827
- [28] Wyatt Z, Joost W, Zhu D and Ankem S 2012 *Int. J. Plast.* **39** 119
- [29] Becker H and Pantleon W 2013 *Comput. Mater. Sci.* **76** 52
- [30] Wang L, Barabash R, Bieler T, Liu W and Eisenlohr P 2013 *Metall. Mater. Trans. A* **44** 3664
- [31] Zharebtsov S, Dyakonov G, Salem A A, Sokolenko V, Salishchev G and Semiatin S 2013 *Acta Mater.* **61** 1167
- [32] Yoo M H and Lee J K 1991 *Phil. Mag. A* **63** 987
- [33] Morris J R, Ye Y and Yoo M H 2005 *Phil. Mag.* **85** 233
- [34] Wang J and Beyerlein I J 2012 *Modelling Simul. Mater. Sci. Eng.* **20** 024002
- [35] Minonishi Y, Ishioka S, Koiwa M and Mobozumi S 1982 *Phys. Status Solidi a* **71** 253
- [36] Lane N, Simak S, Mikhaylushkin A, Abrikosov I, Hultman L and Barsoum M 2011 *Phys. Rev. B* **84** 184101
- [37] Wang J and Beyerlein I J 2012 *Metall. Mater. Trans. A* **43** 3556
- [38] Steyskal E, Oberdorfer B and Sprengel W 2012 *Phys. Rev. Lett.* **108** 055504
- [39] Aksyonov D A, Lipnitskii A G and Kolobov Y R 2012 *Comput. Mater. Sci.* **65** 434
- [40] Conrad H 1981 *Prog. Mater. Sci.* **26** 123
- [41] Baskin Y and Meyer L 1955 *Phys. Rev.* **100** 544
- [42] Lide D R 2003 *Handbook of Chemistry and Physics* (Boca Raton, FL: CRC Press)
- [43] Boureau G and Gerdanian P 1976 *Acta Metall.* **24** 717
- [44] Tetot R, Picard C, Boureau G and Gerdanian P 1978 *J. Chem. Phys.* **69** 326
- [45] Boureau G, Capron N and Tetot R 2008 *Scr. Mater.* **59** 1255
- [46] Hennig R G, Trinkle D R, Bouchet J, Srinivasan S G, Albers R C and Wilkins J W 2005 *Nat. Mater.* **4** 129
- [47] Baranowski B, Majchrzak S and Flanagan T 1971 *J. Phys. F: Met. Phys.* **1** 258
- [48] Thorpe P and Duxbury M F 2002 *Rigidity Theory and Applications* (New York: Springer)
- [49] Du Y A, Ismer L, Rogal J, Hickel T, Neugebauer J and Drautz R 2011 *Phys. Rev. B* **84** 144121
- [50] Kartamyshev A I, Vo D D and Lipnitskii A G 2016 *St. Petersburg Polytechnical Univ. J.: Phys. Math.* at press (doi:10.1016/j.spjpm.2016.05.003)
- [51] Wachowicz A and Kiejna E 2011 *Modelling Simul. Mater. Sci. Eng.* **19** 025001
- [52] Geng W, Freeman A, Wu R, Geller C and Raynolds J 1999 *Phys. Rev. B* **60** 7149
- [53] Janisch R and Elsässer C 2003 *Phys. Rev. B* **67** 224101
- [54] Aydin U, Ismer L, Hickel T and Neugebauer J 2012 *Phys. Rev. B* **85** 155144